Application of Hybrid-Pol SAR in Oil-Spill Detection

Kumar, Ajeet; Mishra, Varsha; Panigrahi, Rajib Kumar; Martorella, Marco

DOI:
10.1109/LGRS.2023.3258224

Application of Hybrid-Pol SAR in Oil-Spill Detection

Ajeet Kumar, *Member, IEEE*, Varsha Mishra, *Member, IEEE*, Rajib Kumar Panigrahi, *Senior Member, IEEE*, and Marco Martorella, *Fellow, IEEE*

***Abstract*— In the application of oil-spill monitoring, the satellite revisit time needs to be as short as possible to identify minor spills before they can cause widespread damage. Simultaneously, it is required to capture a sufficient amount of information about the surface to clearly distinguish between oil-spilled and oil-free sea regions. The hybrid-polarimetry (hybrid-pol) synthetic aperture radar (SAR) system can be exploited for such capabilities. However, limited hybrid-pol-based oil-spill descriptors are reported in the literature in comparison with rich sets of full-polarimetry (full-pol)-based descriptors. In this letter, we establish a direct relation between hybrid-pol data and full-pol data under reflection-symmetry condition. Consequently, through the proposed work, the rich sets of full-pol-based oil-spill descriptors can be derived directly from the hybrid-pol datasets. For the validation of the proposed work, L-band ALOS PALSAR and UAVSAR datasets acquired over the Gulf of Mexico have been used.**

***Index Terms*— Eigenvalue, full polarimetry (full-pol), hybrid polarimetry (hybrid-pol), oil spill, synthetic aperture radar (SAR).**

I. Introduction

IN THIS modern technology era, the country's growth widely depends on oil-based products. Gasoline and heating oil products derived from petroleum provide fuels for automobiles, heat for homes, and useful energy for large and small industrial machinery [1]. As a result, the oil consumption is very high, and its transportation requires large volume tankers and pipelines. Accidents involving tankers, barges, pipelines, refineries, drilling rigs, and storage facilities cause oil spills. Oil spill is one of the most dangerous man-made disasters, which can kill surrounding vegetation, affect marine and coastal ecosystems, affect birds on land, and kill marine mammals (whales, dolphins, and so on) and sea fish. To minimize the impact of oil-polluting events on the ecosystem, it is required to identify minor spills before they cause widespread damage, and further clean them up promptly. The day and night accessibility and almost all-weather capability make synthetic aperture radar (SAR) systems one of the most popular alternatives for monitoring oil-spill detection. SAR provides high resolution along range using a pulse compression technique and along azimuth using Doppler processing concept. The SAR systems established at the initial stage were based on the transmission and reception of a single polarization. The conventional type of single-pol SAR system transmits on one polarization and receives the same (like) polarization. These non-polarimetric SAR systems only acquire scalar information. In order to acquire the maximum possible information about the target, the full-polarimetry (full-pol) SAR architecture has been introduced with the launch of an airborne L-band AIRSAR sensor in 1985. Afterward, for four decades around, full-pol-based SAR has provided promising results in various earth-based monitoring applications. Although full-pol SAR systems can acquire maximum possible information about the target, these systems suffer the drawback of having half swath coverage area in comparison with single-pol SAR systems. This has an adverse impact on the satellite revisit time and, consequently, on oil-spill monitoring applications. To avoid the demerits of full-pol SAR systems associated with swath coverage and to retain the vector information about the target, three configurations of compact-polarimetry (compact-pol): $\pi/4$, dual-circular-pol, and hybrid polarimetry (hybrid-pol) have been introduced in the literature. Among all of these compact-pol configurations, the hybrid-pol mode has been established as an optimum choice due to its simple architecture, independency of the oriented target structures, and negligible co- and cross-polarization interference. The practical implementation of hybrid-pol architecture started with the launch of Mini-SAR on India's lunar Chandrayaan-1 and Mini-RF on NASA's Lunar Reconnaissance Orbiter for planetary exploration. Moreover, for the earth-observing purposes, Indian RISAT-1 and Japanese ALOS-2 were launched in April 2012 and May 2014, respectively. Furthermore, RADARSAT Constellation Mission (RCM) by Canadian space agency, SAOCOM-1 by CONAE, and NISAR jointly by NASA-ISRO are planned to be launched in the near future. The datasets acquired in hybrid-pol mode can usually be implemented in two different ways for the application of oil-spill detection. First, the hybrid-pol oil-spill descriptors can be directly derived from the hybrid-pol Stokes parameters. In this category, a limited number of descriptors reported so far [2], [3], [4], [5]. Second, the pseudo-full-pol information is generated from hybrid-pol data that facilitates to utilize the rich sets of well-established full-pol oil-spill descriptors [6], [7], [8], [9]. The rich number of efficient descriptors also serves well in the supervised way of oil-spill characterization, as the network gets better trained with an increased number of efficient descriptors [10]. This motivated us to explore the second way of exploiting hybrid-pol data for oil-spill detection.

In this work, we proposed a new methodology to generate the pseudo-full-pol information from hybrid-pol measurements. At the outset, a direct relationship is established for

Manuscript received 26 December 2022; revised 30 January 2023; accepted 2 March 2023. Date of publication 16 March 2023; date of current version 19 April 2023. This work was supported by the Radar and Surveillance Systems (RaSS) National Laboratory, National Inter-University Consortium for Telecommunications (CNIT), Pisa, Italy. *(Corresponding author: Ajeet Kumar.)*

Ajeet Kumar is with the Radar and Surveillance Systems (RaSS) National Laboratory, National Inter-University Consortium for Telecommunications (CNIT), 56124 Pisa, Italy (e-mail: ajeet.kumar.in@ieee.org).

Varsha Mishra and Marco Martorella are with the Department of Information Engineering, University of Pisa, 56122 Pisa, Italy.

Rajib Kumar Panigrahi is with the Department of Electronics and Communication Engineering, Indian Institute of Technology Roorkee, Roorkee 247667, India.

Digital Object Identifier 10.1109/LGRS.2023.3258224

exact calculation of $\langle|S_{HV}|^2\rangle$ by overcoming the limitations of reported approaches that either estimated $\langle|S_{HV}|^2\rangle$ through iteration [9], [11], [12] or approximated it as a fraction of backscattered depolarized power [13], [14]. Moreover, by utilizing this $\langle|S_{HV}|^2\rangle$, the remaining pseudo-full-pol elements are calculated. These elements can be further utilized to express the well-established full-pol-based oil-spill descriptors in terms of hybrid-pol elements. We illustrated four full-pol descriptors in this letter and demonstrated their superior performance in separating oil-spilled and clean-sea regions.

This letter is organized as follows. In Section II, we describe the possibility of accurate calculation of $\langle|S_{HV}|^2\rangle$ for oil-spill monitoring and also present the derivation of $\langle|S_{HV}|^2\rangle$ when using hybrid-pol data. Furthermore, by using this information, the full-pol oil-spill descriptors are derived in terms of hybrid-pol parameters in Section III. For the validation of the proposed work, ALOS PALSAR and UAVSAR data containing well-known oil-spilled and clean-sea regions are being used.

II. $\langle|S_{HV}|^2\rangle$ Calculation by Using Hybrid-Pol Data

The $\langle|S_{HV}|^2\rangle$ parameter has great importance in utilizing the rich sets of full-pol-based approaches, even though it is declared as a lost parameter that cannot be exactly calculated using hybrid-pol. This hypothesis came into existence after it was said that even after considering reflection-symmetry condition (which is almost valid for all types of natural surfaces [11]), there are five parameters required to calculate full-pol covariance or coherency matrix, while the hybrid-pol can only acquire four parameters. Both the full-pol information and the hybrid-pol information under reflection-symmetry condition are expressed below in terms of covariance matrices C_{full} and C_{hyb}, respectively

$$C_{\text{full}} = \left\langle \begin{bmatrix} |S_{HH}|^2 & 0 & S_{HH}S_{VV}^* \\ 0 & 2|S_{HV}|^2 & 0 \\ S_{VV}S_{HH}^* & 0 & |S_{VV}|^2 \end{bmatrix} \right\rangle \tag{1}$$

$$C_{\text{hyb}} = \begin{bmatrix} J_{11} & J_{12} \\ J_{12}^* & J_{22} \end{bmatrix} = \frac{1}{2}\left\langle \begin{bmatrix} |S_{HH}|^2 + |S_{HV}|^2 & \iota S_{HH}S_{VV}^* - \iota|S_{HV}|^2 \\ -\iota S_{VV}S_{HH}^* + \iota|S_{HV}|^2 & |S_{VV}|^2 + |S_{HV}|^2 \end{bmatrix} \right\rangle \tag{2}$$

where the symbol $\langle . \rangle$ indicates ensemble averaging. In this letter, we considered right-hand circular polarization (RHCP) transmission-based hybrid-pol architecture. In case of left-hand circular polarization (LHCP) transmission, the ith row and jth column element of C_{hyb} needs to be multiplied with $(-1)^{i+j}$ factor. By comparing the two matrices C_{full} and C_{hyb}, Dubois-Fernandez et al. [15] have stated that "the three real diagonal terms and the real and imaginary parts of one of the nonzero off-diagonal terms," a total of five parameters are required to calculate C_{full}. Similarly, Collins et al. [16] mentioned that after reflection-symmetry consideration, C_{full} "left with five unknowns: $|S_{HH}|^2$, $|S_{VV}|^2$, and $|S_{HV}|^2$ are real, and $S_{HH}S_{VV}^*$ is complex." Yue et al. [17] have also articulated that calculating C_{full} from hybrid-pol is a "problem of estimating five unknowns from four measurements." Furthermore, Espeseth [13] stated that "there are four independent equations with five unknowns" and coined $|S_{HV}|^2$ as a "lost" parameter. In a similar manner, Atteia and Collins [8] stated that the assumption of reflection symmetry "reducing the number of unknowns to five" for C_{full} matrix. Nord et al. [12] stated that each compact-pol mode "reduces to a system of four equations from the covariance matrix and five unknowns" under the assumption of reflection-symmetry condition. Similar statements can be found in [9] and [14], which emphasizes the hypothesis that C_{full} cannot be exactly calculated from C_{hyb}.

We would like to disagree with the previous statements and explain that four instead of five parameters are sufficient to calculate C_{full}. The four parameters are $P_1 = \langle|S_{HV}|^2\rangle$, $P_2 = \langle|S_{HH}|^2\rangle$ or $\langle|S_{VV}|^2\rangle$, $P_3 = \Re(\langle S_{HH}S_{VV}^\star\rangle)$, and $P_4 = \Im(\langle S_{HH}S_{VV}^\star\rangle)$. By using these four parameters, the matrix C_{full} can be expressed as follows:

$$C_{\text{full}} = \left\langle \begin{bmatrix} P_2 & 0 & P_3 + \iota P_4 \\ 0 & 2P_1 & 0 \\ P_3 - \iota P_4 & 0 & \dfrac{{P_3}^2 + {P_4}^2}{P_2} \end{bmatrix} \right\rangle. \tag{3}$$

By observing (3), one can see that there are four unknowns: P_1–P_4, required to estimate the full-pol C_{full} matrix, and the hybrid-pol can also capture the four parameters: J_{11}, J_{22}, $\Re(J_{12})$, and $\Im(J_{12})$, as shown in (2). This motivated us to directly calculate C_{full} from C_{hyb}, and the procedure for doing this is outlined in Sections II-A and II-B. In Section II-A, P_1 or $\langle|S_{HV}|^2\rangle$ is calculated, and further using P_1, the remaining parameters of (3) are calculated in Section II-B.

A. Calculation of $\langle|S_{HV}|^2\rangle$ or P_1 Parameter Using Hybrid-Pol

In the proposed work, we calculate $\langle|S_{HV}|^2\rangle$ or P_1 directly by using the three hybrid-pol-based parameters: sum of hybrid-pol eigenvalues ($\sum_{i=1}^{2}\lambda_i$), multiplication of hybrid-pol eigenvalues ($\prod_{i=1}^{2}\lambda_i$), and hybrid-pol $\Im(J_{12})$ term. In the reported papers, the constant (1/2) in front of C_{hyb} is omitted for the sake of simplicity, as this factor does not impact the polarimetric performance [9], [11], [12]. To keep continuation with the previous work, the factor (1/2) is also omitted here for $\langle|S_{HV}|^2\rangle$ calculation. Based on the eigenvalues' properties, $\sum_{i=1}^{2}\lambda_i$ and $\prod_{i=1}^{2}\lambda_i$ indicate trace and determinant of C_{hyb} matrix, respectively. These two parameters, along with the $\Im(J_{12})$ term [after omitting (1/2) in (2)], can be expressed as follows:

$$\sum_{i=1}^{2}\lambda_i = \left\{\left\langle|S_{HH}|^2\right\rangle + 2\left\langle|S_{HV}|^2\right\rangle + \left\langle|S_{VV}|^2\right\rangle\right\} \tag{4}$$

$$\prod_{i=1}^{2}\lambda_i = \left\langle|S_{HV}|^2\right\rangle\left\{\left\langle|S_{HH}|^2\right\rangle + \left\langle|S_{VV}|^2\right\rangle + 2\Re\left(\left\langle S_{HH}S_{VV}^\star\right\rangle\right)\right\} \tag{5}$$

$$\Im(J_{12}) = \left\{\Re\left(\left\langle S_{HH}S_{VV}^\star\right\rangle\right) - \left\langle|S_{HV}|^2\right\rangle\right\}. \tag{6}$$

By putting the information of (4) into (5), we get

$$\prod_{i=1}^{2}\lambda_i = \left\langle|S_{HV}|^2\right\rangle\left\{\sum_{i=1}^{2}\lambda_i - 2\left\langle|S_{HV}|^2\right\rangle + 2\Re\left(\left\langle S_{HH}S_{VV}^\star\right\rangle\right)\right\}. \tag{7}$$

Furthermore, by using (6) in (7), $\langle|S_{HV}|^2\rangle$ can be written as follows:

$$\left\langle|S_{HV}|^2\right\rangle = \frac{\prod_{i=1}^{2}\lambda_i}{\sum_{i=1}^{2}\lambda_i + 2\Im(J_{12})}. \tag{8}$$

Through (8), it is possible now to calculate $\langle|S_{HV}|^2\rangle$ by using hybrid-pol data as λ_i, and $\Im(J_{12})$ both can be calculated from hybrid-pol information expressed in (2).

B. Calculation of P_2–P_4 Parameters Using Hybrid-Pol

Using P_1 or $\langle|S_{HV}|^2\rangle$ and hybrid-pol covariance matrix elements [as shown in (2)], the remaining parameters P_2–P_4 can be calculated. The expressions for P_1–P_4 can be summarized as follows:

$$P_1 = \frac{\prod_{i=1}^{2}\lambda_i}{\sum_{i=1}^{2}\lambda_i + 2\Im(J_{12})} \tag{9}$$

$$P_2 = 2J_{11} - P_1 \tag{10}$$

$$P_3 = 2\Im(J_{12}) + P_1 \tag{11}$$

$$P_4 = -2\Re(J_{12}). \tag{12}$$

From (9)–(12), it is confirmed that parameters P_1–P_4 can be calculated by using only hybrid-pol information, and further by using these parameters, the matrix C_{full} can be computed from (3). Moreover, from (10)–(12), one can see that the accuracy in computation of parameters P_2–P_4 certainly depends on an accurate calculation of P_1 from hybrid-pol. Validation of parameter P_1, and the utilization of these P_1–P_4 parameters in oil-spill detection, is carried out in Section III.

III. Result Analysis and Validation

To properly validate parameter P_1 or $\langle|S_{HV}|^2\rangle$, generated from the proposed expression derived in (8), we use hybrid-pol data synthesized from full-pol ALOS PALSAR (data ID: ALPSRP104460550) and UAVSAR (data ID: gulfco_32010) datasets. This synthesis process is described in [13] and [18]. The selected datasets cover the well known oil-spilled and clean-sea regions in the Gulf of Mexico [19], [20] and possess high range (slant) × azimuth resolutions of 9.5 m × 4.5 m and 1.7 m × 1 m, respectively. In the entire region of selected datasets, the targets that are eminent in violating reflection-symmetry conditions (such as oriented dihedral or man-made complex structures) are absent. During these ALOS PALSAR and UAVSAR data acquisitions, the local wind speeds were around 4–8 and 2.5–8.5 m/s, respectively, satisfying the low-to-moderate wind condition, and the incidence angles (central) were 23.89° and 43.5°, respectively, satisfying the intermediate-incidence-angle condition. These two conditions are optimal for the purpose of oil-spill detection [19], [20], [21]. Before carrying out the analyses through the considered datasets, radiometric calibration is performed, and the required multilooking of the datasets is carried out to obtain the square-pixel spacing in the output image. Furthermore, for the speckle reduction, both the datasets are filtered with a Refined-Lee filter [22]. The SPAN images of both the datasets are shown in Fig. 1 for the reference.

A. Validation of Hybrid-Pol-Based $\langle|S_{HV}|^2\rangle$ Generation

For performance validation, the normalized $\langle|S_{HV}|^2\rangle$ values generated using hybrid-pol data are compared with that of the original full-pol data. These normalized values can be given as follows:

$$\langle|S_{HV}|^2\rangle_{\text{hyb}} = \frac{P_1}{J_{11}+J_{22}} \tag{13}$$

$$\langle|S_{HV}|^2\rangle_{\text{full}} = \frac{C_{22}}{C_{11}+C_{22}+C_{33}} \tag{14}$$

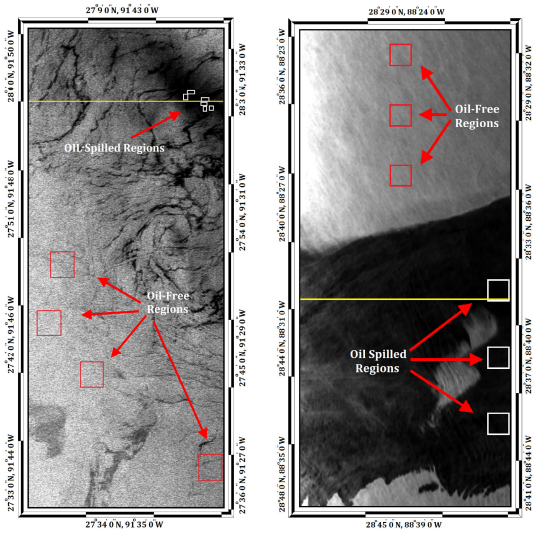

(a) (b)

Fig. 1. SPAN image of (a) ALOS PALSAR data (data ID: ALPSRP104460550) and (b) UAVSAR data (data ID: gulfco_32010).

where J_{ij} and C_{ij} correspond to the ith row and jth column of hybrid-pol and full-pol covariance matrix elements, respectively. The $\langle|S_{HV}|^2\rangle_{\text{hyb}}$ calculated entirely using hybrid-pol data is expected to have similar value of $\langle|S_{HV}|^2\rangle_{\text{full}}$ (calculated using full-pol data), subject to perfect retrieval of P_1 or $\langle|S_{HV}|^2\rangle$ through the proposed approach. Therefore, to visualize the reconstruction performance of the proposed method over entire regions of implemented ALOS PALSAR and UAVSAR datasets [for the whole area depicted in Fig. 1(a) and (b)], parameters $\langle|S_{HV}|^2\rangle_{\text{hyb}}$ and $\langle|S_{HV}|^2\rangle_{\text{full}}$ are shown in Fig. 2(a) and (b), respectively, for ALOS PALSAR data, and in Fig. 2(c) and (d), respectively, for UAVSAR data. One can observe that for both the datasets, the images of $\langle|S_{HV}|^2\rangle_{\text{hyb}}$ and $\langle|S_{HV}|^2\rangle_{\text{full}}$ exhibit almost similar information, and more specifically, similar extent of oil-based features over the surface is visible in both of the images. To carry out more clear and pixel-to-pixel comparison, transects on both datasets are taken under consideration. These transects are shown with yellow lines in Fig. 1(a) and (b) for ALOS PALSAR and UAVSAR datasets, respectively. For these single-row-based transects, $\langle|S_{HV}|^2\rangle_{\text{hyb}}$ and $\langle|S_{HV}|^2\rangle_{\text{full}}$ are plotted in Fig. 2(e) and (f). The corresponding plots verify that $\langle|S_{HV}|^2\rangle_{\text{hyb}}$ and $\langle|S_{HV}|^2\rangle_{\text{full}}$ show similar variations in oil-free or oil-spilled regions, and the blue line indicating hybrid-pol-based information, more or less follows the red line indicating full-pol-based information for both the datasets. To evaluate the error in $\langle|S_{HV}|^2\rangle_{\text{hyb}}$ retrieval over the entire regions of implemented ALOS PALSAR and UAVSAR datasets, the median (M) and standard deviation (SD) of the relative error function $E_r = \{\langle|S_{HV}|^2\rangle_{\text{full}} - \langle|S_{HV}|^2\rangle_{\text{hyb}}\}/\langle|S_{HV}|^2\rangle_{\text{full}}$ are calculated and presented in Table I. The results are compared with Souyris' iterative-based approach [11] and Espeseth's eigenvalue-based approach [13], [14]. It is worth observing that the median values are much closer to zero in case of the proposed method. This indicates a better retrieval of $\langle|S_{HV}|^2\rangle$ by the proposed approach.

B. Full-Pol-Based Oil-Spill Descriptors Derived in Terms of Hybrid-Pol Parameters

As the full-pol matrix C_{full} can now be calculated by using hybrid-pol information, the full-pol oil-spill descriptors

TABLE I
MEDIAN (M) AND STANDARD DEVIATION (SD) OF E_r

Methods / Datasets	Souyris' method		Espeseth's method		Proposed method	
ALOS PALSAR	M	0.1523	M	0.0649	M	0.0589
	SD	0.0409	SD	0.0396	SD	0.0400
UAVSAR	M	0.1600	M	0.0167	M	-0.0066
	SD	0.0476	SD	0.0223	SD	0.0309

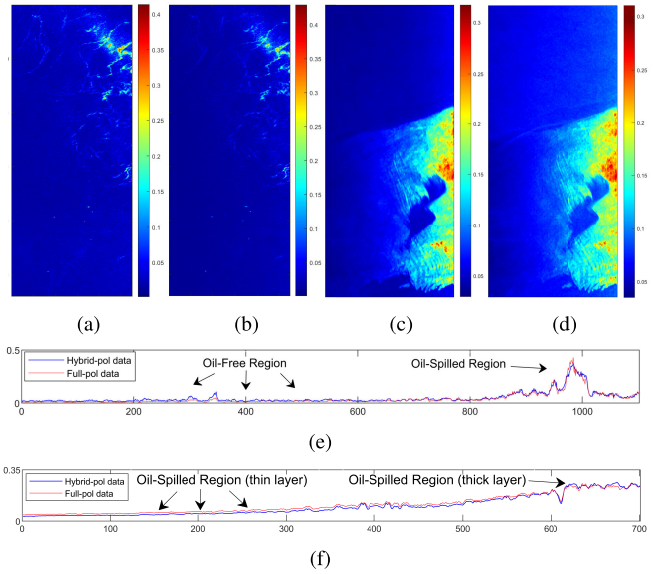

Fig. 2. (a) and (c) $\langle |S_{HV}|^2 \rangle_{\text{hyb}}$ generated for ALOS PALSAR and UAVSAR data, respectively. (b) and (d) $\langle |S_{HV}|^2 \rangle_{\text{full}}$ generated for ALOS PALSAR and UAVSAR data, respectively. $\langle |S_{HV}|^2 \rangle_{\text{hyb}}$ and $\langle |S_{HV}|^2 \rangle_{\text{full}}$ plotted along single row transects for ALOS PALSAR and UAVSAR datasets are shown in (e) and (f), respectively.

can directly be calculated by using hybrid-pol parameters. Consequently, we have derived a few popular and widely used full-pol oil-spill descriptors in terms of parameters P_1–P_4, and from (8)–(12), we know that these parameters can be calculated based on hybrid-pol information.

1) Real Part of Co-Polarization Cross Product ($|\Re(\langle S_{HH} S_{VV}^{\star} \rangle)|$): Parameter $|\Re(\langle S_{HH} S_{VV}^{\star} \rangle)|$ is related to the scattering behavior of the target that increases when moving from oil-covered to clean-sea surface area. This multipolarization parameter has proved to be optimal in separating biogenic slicks and mineral oil types [23]. In terms of hybrid-pol parameter, $|\Re(\langle S_{HH} S_{VV}^{\star} \rangle)|$ can be expressed as follows:

$$\left|\Re\left(\left\langle S_{HH} S_{VV}^{\star} \right\rangle\right)\right| = |P_3|. \tag{15}$$

2) Mueller Scattering Matrix Element (M_{33}): The Mueller scattering matrix element ($M_{33} = M_{33}^{\text{I}} + M_{33}^{\text{II}}$) can be exploited to detect mineral oil slicks and distinguish them from biogenic look-alikes [24]. In terms of hybrid-pol parameters, M_{33} can be expressed as follows:

$$M_{33} = \Re\left(\left\langle S_{HH} S_{VV}^{\star} \right\rangle\right) + \left\langle |S_{HV}|^2 \right\rangle = P_3 + P_1. \tag{16}$$

M_{33}^{I} indicates correlation between co-polarized channels, which is expected to be high in clean sea region and low in oil-spilled region. Contrarily, M_{33}^{II} has lower values in clean-sea regions and comparatively higher values in oil-spilled regions. Therefore, $|M_{33}^{\text{I}}| > M_{33}^{\text{II}}$ in clean-sea regions and $|M_{33}^{\text{I}}| < M_{33}^{\text{II}}$ in oil-spilled regions. By exploiting these relations, the ratio of $|M_{33}^{\text{I}}|$ to M_{33}^{II} can be used as an oil-spill descriptor [24].

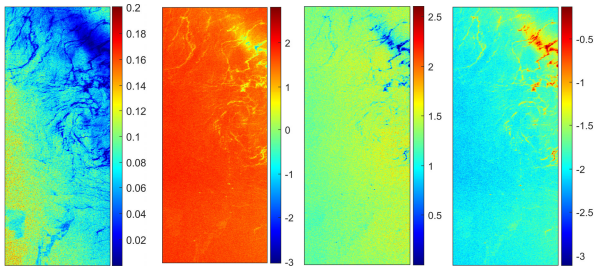

Fig. 3. Plots of oil-spill descriptors derived using hybrid-pol parameters for ALOS PALSAR dataset. (a) $|\Re(\langle S_{HH} S_{VV}^{\star} \rangle)|$. (b) Log of $|M_{33}^{\text{I}}|/M_{33}^{\text{II}}$. (c) γ_{CO}. (d) Log of P_X.

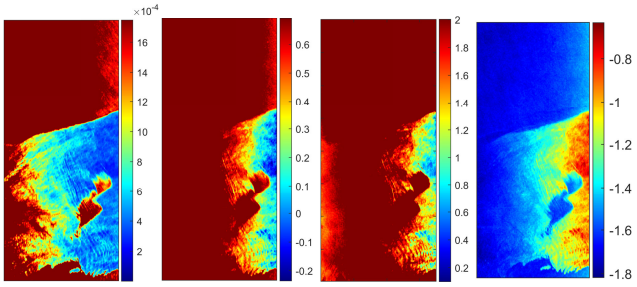

Fig. 4. Plots of oil-spill descriptors derived using hybrid-pol parameters for the UAVSAR dataset. (a) $|\Re(\langle S_{HH} S_{VV}^{\star} \rangle)|$. (b) Log of $|M_{33}^{\text{I}}|/M_{33}^{\text{II}}$. (c) γ_{CO}. (d) Log of P_X.

3) Co-Polarization Ratio (γ_{CO}): The co-polarization ratio (γ_{CO}) is a function of the dielectric constant that is not affected by ocean-wave surface roughness [25]. As the clean sea has a much higher dielectric constant of around $80 - 70\iota$ compared with the oil-spilled regions with a dielectric constant of around $2.3 - 0.02\iota$, parameter γ_{CO} can discriminate the oil-spilled regions from clean-sea regions. In terms of hybrid-pol parameters, γ_{CO} can be expressed as follows:

$$\gamma_{\text{CO}} = \frac{\left\langle |S_{VV}|^2 \right\rangle}{\left\langle |S_{HH}|^2 \right\rangle} = \frac{P_3^2 + P_4^2}{P_2^2}. \tag{17}$$

4) Cross-Polarization Ratio (P_X): The oil-spilled and oil-free regions are expected to generate higher and lower value of cross-polarization ratio (P_X), respectively [21]. In terms of hybrid-pol parameters, P_X can be expressed as follows:

$$P_X = \frac{\left\langle |S_{HV}|^2 \right\rangle}{\left\langle |S_{HH}|^2 \right\rangle + \left\langle |S_{VV}|^2 \right\rangle} = \frac{P_1 P_2}{P_2^2 + P_3^2 + P_4^2}. \tag{18}$$

The Medians (M) and the corresponding Standard Deviations (SDs) of the aforesaid parameters are calculated and shown separately for the ALOS PALSAR and UAVSAR datasets in Table II for the oil-spilled and oil-free regions, marked with white and red rectangles, respectively, in Fig. 1(a) and (b). To evaluate the separability between two classes of oil-spilled and oil-free, we implemented Jeffries–Matusita (JM) separability distance here that can be expressed as $\text{JM} = 2(1 - e^{-\text{BD}})$, where BD indicates Bhattacharya distance [21]. The parameter JM has been proven to be useful in separating oil-spilled and oil-free classes based on various features [21]. JM values ranging from 0 to 2 indicate an increase in the separation capability of features, where 0 and 2 indicate minimum and

TABLE II
PERFORMANCE OF OIL-SPILL DESCRIPTORS USING ALOS PALSAR AND UAVSAR DATASETS

Full-pol oil-spill descriptors derived in terms of hybrid-pol	ALOS PALSAR					UAVSAR				
	Oil-Spilled		Oil-Free		JM	Oil-Spilled		Oil-Free		JM
$\lvert\Re(\langle S_{HH}S_{VV}^{\star}\rangle)\rvert$	M	0.0007	M	0.0886	1.9824	M	0.0002	M	0.0017	2
	SD	0.0013	SD	0.0230		SD	4.7×10^{-5}	SD	0.0001	
Mueller scattering matrix element (*log* of $\lvert M_{33}^{\mathrm{I}}\rvert/M_{33}^{\mathrm{II}}$)	M	-0.2831	M	1.6814	1.9017	M	-0.0344	M	0.6582	2
	SD	0.5745	SD	0.1658		SD	0.0751	SD	0.0209	
Co-Polarization ratio	M	0.0818	M	1.3415	1.9992	M	0.4680	M	1.9943	2
	SD	0.0012	SD	0.0231		SD	4.8×10^{-5}	SD	0.0002	
log of Cross-polarization Ratio	M	-0.4094	M	-1.9881	2	M	-0.9280	M	-1.6725	2
	SD	0.1621	SD	0.1642		SD	0.0967	SD	0.0214	

maximum separation, respectively. Moreover, the JM values greater than 1.9, ranging in between 1 and 1.9, and less than 1, indicate strong, good, and weak separabilities between oil-spilled and oil-free regions, respectively. Hence, based on the results shown in Table II, all the derived descriptors provide strong separability. Furthermore, it is worth noting that the descriptors perform better in case of UAVSAR data, in comparison with ALOS PALSAR. The possible reason for this lies in the fact that the UAVSAR data have lower noise floor than ALOS PALSAR [20]. The complete image plots of all the derived descriptors corresponding to ALOS PALSAR and UAVSAR datasets are shown in Figs. 3 and 4, respectively. In the images, a clear contrast between oil-spilled and oil-free regions can be seen for almost all the descriptors.

IV. CONCLUSION

It has been established in this work that there are actually four unknowns instead of five required to generate full-pol information after imposing reflection symmetry condition. Expressions for these unknowns have been derived using hybrid-pol data. Consequently, the work presented in this letter facilitates to derive full-pol-based oil-spill descriptors in terms of hybrid-pol data. For validation, the four oil-spill descriptors are derived entirely using hybrid-pol information. Based on the JM separability criterion, it has been shown that all the derived oil-spill descriptors provide very strong separability between oil-spilled and oil-free regions. The future extension of this work could be analyzing more of such oil-spill descriptors that can be further implemented to separate biogenic look-alikes with the mineral oil spills.

REFERENCES

[1] U. S. Environmental Protection Agency. (Dec. 1999). *Understanding Oil Spills and Oil Spill Response*. Office Emergency Remedial Response. [Online]. Available: https://www.epa.gov

[2] R. Shirvany, M. Chabert, and J. Y. Tourneret, "Ship and oil-spill detection using the degree of polarization in linear and hybrid/compact dual-pol SAR," *IEEE J. Sel. Topics Appl. Earth Observ. Remote Sens.*, vol. 5, no. 3, pp. 885–892, Jun. 2012.

[3] J. Yin, J. Yang, Z.-S. Zhou, and J. Song, "The extended Bragg scattering model-based method for ship and oil-spill observation using compact polarimetric SAR," *IEEE J. Sel. Topics Appl. Earth Observ. Remote Sens.*, vol. 8, no. 8, pp. 3760–3772, Aug. 2015.

[4] A. Buono, F. Nunziata, M. Migliaccio, and X. Li, "Polarimetric analysis of compact-polarimetry SAR architectures for sea oil slick observation," *IEEE Trans. Geosci. Remote Sens.*, vol. 54, no. 10, pp. 5862–5874, Oct. 2016.

[5] H. Li, W. Perrie, Y. He, J. Wu, and X. Luo, "Analysis of the polarimetric SAR scattering properties of oil-covered waters," *IEEE J. Sel. Topics Appl. Earth Observ. Remote Sens.*, vol. 8, no. 8, pp. 3751–3759, Aug. 2015.

[6] X. Wang, Y. Shao, F. Zhang, and W. Tian, "Comparison of C- and L-band simulated compact polarized SAR in oil spill detection," *Frontiers Earth Sci.*, vol. 13, no. 2, pp. 351–360, Jun. 2019.

[7] J. Yin, W. Moon, and J. Yang, "Model-based pseudo-quad-pol reconstruction from compact polarimetry and its application to oil-spill observation," *J. Sensors*, vol. 2015, Jul. 2015, Art. no. 734848.

[8] G. E. Atteia and M. J. Collins, "On the use of compact polarimetry SAR for ship detection," *ISPRS J. Photogramm. Remote Sens.*, vol. 80, pp. 1–9, Jun. 2013.

[9] M. J. Collins et al., "On the use of simulated airborne compact polarimetric SAR for characterizing oil–water mixing of the deepwater horizon oil spill," *IEEE J. Sel. Topics Appl. Earth Observ. Remote Sens.*, vol. 8, no. 3, pp. 1062–1077, Mar. 2015.

[10] D. Song, Y. Ding, X. Li, B. Zhang, and M. Xu, "Ocean oil spill classification with RADARSAT-2 SAR based on an optimized wavelet neural network," *Remote Sens.*, vol. 9, no. 8, p. 799, Aug. 2017.

[11] J.-C. Souyris et al., "Compact polarimetry based on symmetry properties of geophysical media: The $\pi/4$ mode," *IEEE Trans. Geosci. Remote Sens.*, vol. 43, no. 3, pp. 634–646, Mar. 2005.

[12] M. E. Nord, T. L. Ainsworth, J. S. Lee, and N. J. S. Stacy, "Comparison of compact polarimetric synthetic aperture radar modes," *IEEE Trans. Geosci. Remote Sens.*, vol. 47, no. 1, pp. 174–188, Jan. 2009.

[13] M. M. Espeseth, "Synthetic aperture radar compact polarimetry for sea ice surveillance," M.S. thesis, Fac. Sci. Technol., Arctic Univ. Norway, Tromsø, Norway, 2015.

[14] A. Kumar, A. Das, and R. K. Panigrahi, "Hybrid-pol decomposition methods: A comparative evaluation and a new entropy-based approach," *IETE Tech. Rev.*, vol. 37, no. 3, pp. 296–308, May 2020.

[15] P. C. Dubois-Fernandez, J. C. Souyris, S. Angelliaume, and F. Garestier, "The compact polarimetry alternative for spaceborne SAR at low frequency," *IEEE Trans. Geosci. Remote Sens.*, vol. 46, no. 10, pp. 3208–3222, Oct. 2008.

[16] M. J. Collins, M. Denbina, and G. Atteia, "On the reconstruction of quad-Pol SAR data from compact polarimetry data for ocean target detection," *IEEE Trans. Geosci. Remote Sens.*, vol. 51, no. 1, pp. 591–600, Jan. 2013.

[17] D. Yue, F. Xu, and Y. Jin, "Wishart–Bayesian reconstruction of quad-pol from compact-pol SAR Image," *IEEE Geosci. Remote Sens. Lett.*, vol. 14, no. 9, pp. 1623–1627, Sep. 2017.

[18] R. K. Raney, "Hybrid-polarity SAR architecture," *IEEE Trans. Geosci. Remote Sens.*, vol. 45, no. 11, pp. 3397–3404, Nov. 2007.

[19] M. Migliaccio, F. Nunziata, A. Montuori, X. Li, and W. G. Pichel, "A multifrequency polarimetric SAR processing chain to observe oil fields in the Gulf of Mexico," *IEEE Trans. Geosci. Remote Sens.*, vol. 49, no. 12, pp. 4729–4737, Dec. 2011.

[20] C. E. Jones et al., *Studies of the Deepwater Horizon Oil Spill With the UAVSAR Radar*. Washington, DC, USA: American Geophysical Union (AGU), 2011, pp. 33–50.

[21] G. Li et al., "Marine oil slick detection based on multi-polarimetric features matching method using polarimetric synthetic aperture radar data," *Sensors*, vol. 19, no. 23, p. 5176, 2019.

[22] J. S. Lee and E. Pottier, *Polarimetric Radar Imaging: From Basics to Applications*. Boca Raton, FL, USA: CRC Press, 2009.

[23] S. Skrunes, C. Brekke, and T. Eltoft, "Characterization of marine surface slicks by RadarSat-2 multipolarization features," *IEEE Trans. Geosci. Remote Sens.*, vol. 52, no. 9, pp. 5302–5319, Sep. 2014.

[24] F. Nunziata, A. Gambardella, and M. Migliaccio, "On the Mueller scattering matrix for SAR sea oil slick observation," *IEEE Geosci. Remote Sens. Lett.*, vol. 5, no. 4, pp. 691–695, Oct. 2008.

[25] B. Minchew, C. E. Jones, and B. Holt, "Polarimetric analysis of backscatter from the deepwater horizon oil spill using L-band synthetic aperture radar," *IEEE Trans. Geosci. Remote Sens.*, vol. 50, no. 10, pp. 3812–3830, Oct. 2012.

Open Access funding provided by 'Università di Pisa' within the CRUI CARE Agreement